

Structural-acoustic optimization of a pressurized, ribbed panel

Micah R Shepherd and Stephen A Hambric

Citation: *Proc. Mtgs. Acoust.* **22**, 065003 (2014); doi: 10.1121/2.0000045

View online: <https://doi.org/10.1121/2.0000045>

View Table of Contents: <https://asa.scitation.org/toc/pma/22/1>

Published by the [Acoustical Society of America](#)

ARTICLES YOU MAY BE INTERESTED IN

[Ultrasonic scattering from poroelastic materials using a mixed displacement-pressure formulation](#)

Proceedings of Meetings on Acoustics **22**, 045002 (2014); <https://doi.org/10.1121/2.0000063>

[Stethoscope-based detection of detorqued bolts using impact-induced acoustic emissions](#)

Proceedings of Meetings on Acoustics **22**, 065001 (2014); <https://doi.org/10.1121/2.0000013>

[Using arrays of air-filled resonators to attenuate low frequency underwater sound](#)

Proceedings of Meetings on Acoustics **22**, 045004 (2014); <https://doi.org/10.1121/2.0000145>

[Numerical simulations of an electromagnetic actuator in a low-frequency range for dipole acoustic wave logging](#)

Proceedings of Meetings on Acoustics **22**, 045001 (2014); <https://doi.org/10.1121/2.0000031>

[The impact of crossfit training-weight drops on floating floors](#)

Proceedings of Meetings on Acoustics **22**, 065002 (2014); <https://doi.org/10.1121/2.0000014>

[Prediction of flow induced sound and vibration of periodically stiffened plates](#)

The Journal of the Acoustical Society of America **133**, 146 (2013); <https://doi.org/10.1121/1.4768875>



**Advance your science and career
as a member of the**

ACOUSTICAL SOCIETY OF AMERICA

LEARN MORE





168th Meeting of the Acoustical Society of America

Indianapolis, Indiana

27-31 October 2014

Structural Acoustics and Vibration: Paper 2aSAb1

Structural-acoustic optimization of a pressurized, ribbed panel

Micah R. Shepherd and **Stephen A. Hambric**

*The Pennsylvania State University, Applied Research Laboratory / Graduate Program
in Acoustics, University Park, PA; mrs30@psu.edu; sah19@psu.edu*

A method to reduce the noise radiated by a ribbed panel excited by turbulent boundary layer flow is presented. To compute the structural-acoustic response, a modal approach based on finite element / boundary element analysis was coupled to a turbulent boundary flow forcing function. A static pressure load was also applied to the panel to simulate cabin pressurization during flight. The radiated sound power was then minimized by optimizing the horizontal and vertical rib location and rib cross section using an evolutionary search algorithm. Nearly 10 dB of reduction was achieved by pushing the ribs to the edge of the panel.



1 Introduction

There are many modern applications where noise reduction or vibration control is needed. Low noise and vibration levels are often required to ensure vehicle or payload integrity, passenger comfort or low environmental impact. Because of these noise and vibration requirements, modeling techniques are used to predict or simulate levels for new or modified designs so that requirements can be met in the design stage. Such simulations often require numerical tools such as Finite Element (FE) Analysis or Boundary Element (BE) Analysis. Realistic drive forces and constraints must then be coupled to the FE/BE analysis in order to complete an accurate simulation. If the noise or vibration levels do not meet a given requirement, the model must then be altered or adjusted to improve the design. Structural-acoustic optimization procedures can be well suited to optimize a structure for low noise, vibration or other desired acoustic behavior (Belegundu et al. 1994)(Marburg et al. 2006)(Johnson and Cunefare 2007)(Naghshineh et al. 1992).

This paper presents the structural-acoustic optimization of a mock aircraft panel in order to minimize the radiated power. Rib locations and cross-sectional area are used as the design variables during optimization and a turbulent boundary layer flow model is used to as the forcing function. A static pressure load is also applied to the panel to simulate cabin pressurization during flight. Nearly 10 dB of reduction is achieved by pushing the ribs to the edge of the panel.

2 Methods

2.1 Structural-acoustic Analysis

The vibration response of a structure can be determined efficiently using a summation of normal modes as there are typically far fewer modes than physical points. The mode shapes and natural frequencies can be found by solving the eigenvalue problem

$$(\mathbf{K} - \omega^2 \mathbf{M})\phi = 0, \quad (1)$$

where \mathbf{M} is the mass matrix and \mathbf{K} is the stiffness matrix. The modal velocity transfer function matrix is then obtained using

$$\mathbf{h}(\omega) = j\omega [-\omega^2 \mathbf{m} + j\omega \mathbf{b} + \mathbf{k}]^{-1}. \quad (2)$$

In Eq. 2, $\mathbf{m} = \phi^T \mathbf{M} \phi$ is the modal mass, $\mathbf{b} = \phi^T \mathbf{B} \phi$ is the modal damping and $\mathbf{k} = \phi^T \mathbf{K} \phi$ is the modal stiffness. When the mode shapes are mass-normalized, the modal mass matrix becomes the identity matrix and the modal stiffness matrix becomes a diagonal of eigenvectors, ω_n^2 .

To accommodate these computations in modal coordinates, the modal forcing function matrix, G_{FF} can be transformed to modal space by being pre- and post- multiplied by the mode shapes. G_{FF} can be any stochastic excitation that is stationary and ergodic so that modal force matrix, G_{ff} , describes the coupling between any matrix of external forces and the vibration modes. More generally, G_{ff} represents the modal acceptance of energy matrix and can be rewritten in the form

$$G_{ff} = \int \int_S \phi_i \phi_j G_{FF} dS, \quad (3)$$

which resembles the joint acceptance function.(Powell 1958) In order to preserve the physical meaning of the coupling between the force and the structure, G_{ff} was used instead of the joint acceptance function.

Table 1: TBL flow parameters

Density (ρ)	1000 kg/m ³
Friction Velocity (u_τ)	0.1542 m/s
Free-stream Velocity (U)	5.14 m/s (10 knots)
Convective Velocity (U_c)	3.598 m/s
Boundary Layer Disp Thickness (δ^*)	0.0022 m
Kinematic Viscosity (ν)	1.15e-6
Stream-wise Decay Constant (β_1)	0.11
Span-wise Decay Constant (β_2)	0.7
Turbulence Constant ($\hat{\alpha}$)	0.12

The modal amplitudes caused by the forcing function can now be computed to form a modal response cross-spectral density (CSD) matrix

$$\mathbf{G}_{\psi\psi} = \mathbf{h}(\omega)\mathbf{G}_{ff}\mathbf{h}(\omega)^H. \quad (4)$$

This is the modal equivalent of the multiple input multiple output problem (in matrix form) found in Bendat and Piersol.(Bendat and Piersol 2000) The modal amplitude CSD matrix represents the amount of forcing function energy accepted by each mode such that reducing $\mathbf{G}_{\psi\psi}$ will subsequently reduce structural vibration and radiation.

The radiated sound power spectral density can be computed, given the resistance matrix R is known, using

$$G_{P_{rad}} = \sum_{m=1}^M \sum_{n=1}^M r_{mn} \mathbf{G}_{\psi_m\psi_n}, \quad (5)$$

where $r_{mn} = \phi_m^T R \phi_n$ is the modal resistance matrix and M is the number of retained modes. This analysis procedure has been used to predict TBL-induced acoustic power sources in elbowed pipes(Hambric et. al 2010) and optimize the radiation of a curved underwater panel(Shepherd and Hambric 2014). The modal resistance matrix was computed using the lumped parameter boundary element method.(Koopmann and Fahnlne 1997)

2.2 Turbulent Boundary Layer Forcing Function

The forcing function matrix for turbulence-induced wall pressures resulting from flow over a structure can be computed using the product of a pressure auto-spectrum (φ) and a pressure cross-spectrum function (Γ).

$$G_{FF} = \varphi(\omega)\Gamma(\vec{r}, \omega) \quad (6)$$

The point pressure spectrum $\varphi(\omega)$ sets the amplitude of the force and depends on the flow conditions. The pressure spectrum used in the research was a modified version of the Chase model(Lysak 2006) defined as

$$\varphi(\omega) = \frac{3\rho^2 u_\tau^4}{f^*} \left[\frac{(f/f^*)^2}{\{(f/f^*)^2 + \hat{\alpha}^2\}^{3/2}} \right] e^{-14f\nu/u_\tau^2}, \quad (7)$$

where f is the frequency, $f^* = U/2/\pi/\delta^*$ and all other variables are defined in Table 1.

The cross-spectrum Γ defines the partially-correlated regions of pressure over the structure and is often referred to as a coherence function. A well-known TBL coherence function model was proposed by Corcos(Corcos 1963) as

$$\Gamma(\xi_1, \xi_2, \omega) = e^{-\alpha_1|\omega\xi_1/U_c|}e^{-\alpha_2|\omega\xi_2/U_c|}e^{j\omega\xi_1/U_c}, \quad (8)$$

where ξ is the separation distance (the streamwise direction denoted with subscript 1 and spanwise with subscript 2) between points x_μ and x_ν , α is the decay constant (streamwise and spanwise) and U_c is the convective flow velocity. The convective wavenumber can be defined as $k_c = \omega/U_c$. Although the Corcos model is often used in the literature due to its relative simplicity, it has been shown to overpredict low-wavenumber energy. To correct this, Mellen(Mellen 1990) suggested the following TBL model:

$$\Gamma(\xi_1, \xi_2, \omega) = e^{-\sqrt{(\alpha_1|\omega\xi_1/U_c|)^2+(\alpha_2|\omega\xi_2/U_c|)^2}}e^{j\omega\xi_1/U_c}. \quad (9)$$

The Mellen model maintains the exponential model of Corcos but couples the streamwise and spanwise components in the decay, which smooth out the low wavenumber behavior.

2.3 Pressurization

Often structural panels have an external load applied to them, such as cabin pressurization of an aircraft panel. This will change the stiffness of the structure and create different vibration behavior. For flat plates, this is often accounted for by including the in-plane tension in the governing equations, since the load deflection effectively induces curvature into the system. The in-plane tension gives the panel more stiffness and therefore increases wavespeeds and natural frequencies.

To include any preload effects in the analysis procedure described previously, the normal modes must be computed when the load is present. Eigenvalue analysis can be performed on the total stiffness matrix which is a summation of the geometric stiffness matrix and the differential (or structural) stiffness. The differential stiffness comes from performing a static solution with the specified loads. In the finite element software NASTRAN, the static load is computed in a separate subcase and the STATSUB command is used in the subcase with the eigenvalue analysis.

2.4 Optimization Loop

For low frequency noise reduction, the radiated sound power was computed up to 500 Hz. The total sound power was then computed as used as the objective function to be minimized. The optimization algorithm that was used for this research was a real-valued evolutionary strategy with covariance matrix adaption (CMA-ES) developed by Hansen.(Hansen 2006) The algorithm adapts the covariance matrix of a proposed set of solutions to favor the solutions with the best fitness value. The covariance matrix is initially populated with a defined number of candidate solutions which are distributed about a mean value. This distribution is then adapted based on the fitness of each solution and their respective distance from the mean. New candidate solutions are sampled according to the multivariate distribution and the process is repeated until a stop criterion is reached. For a convex-quadratic function, the covariance matrix will adaptively estimate the inverse Hessian matrix and thus is similar to the quasi-Newton gradient-based method. However, the design space is not confined to any particular geometrical condition (i.e. convex or concave). CMAES is also known to have several invariance properties.(Hansen 2006)

3 Ribbed Panel

Since TBL-induced noise is the dominant contributor to interior aircraft noise when flying at cruise conditions, it can be valuable to design fuselage panels which will inefficiently accept and radiate noise into the fuselage. Structural-acoustic optimization was performed on a rib-stiffened panel that represents a notional fuselage section of a commercial aircraft. The panel is 0.9433 m by 0.84 m by 15 mm with the panel edges (up to 4 cm) thickened by 15 mm. The panel has two ringframes and three stringers with the frames oriented perpendicular to the flow direction and the stringers parallel to the flow direction, creating twelve subpanel areas. The baseline design with approximately equispaced ribs is shown in Fig. 1 with the normalized rib center location notated.

A finite element model was created using linear solid elements with material properties of aluminum (see Table 2). The base plate has two elements through the thickness with simply supported boundary conditions applied to the middle nodes (along the neutral axis). The plate has 94 elements in the flow direction and 84 elements in the cross-flow direction so that the element surface dimensions are 1.0035 cm x 1.0 cm. The edge of the panel was thickened to push the ribs away from the edge of the panel. The thickened edge has just one element on top of the base elements making the total number of baseplate elements 17,152.

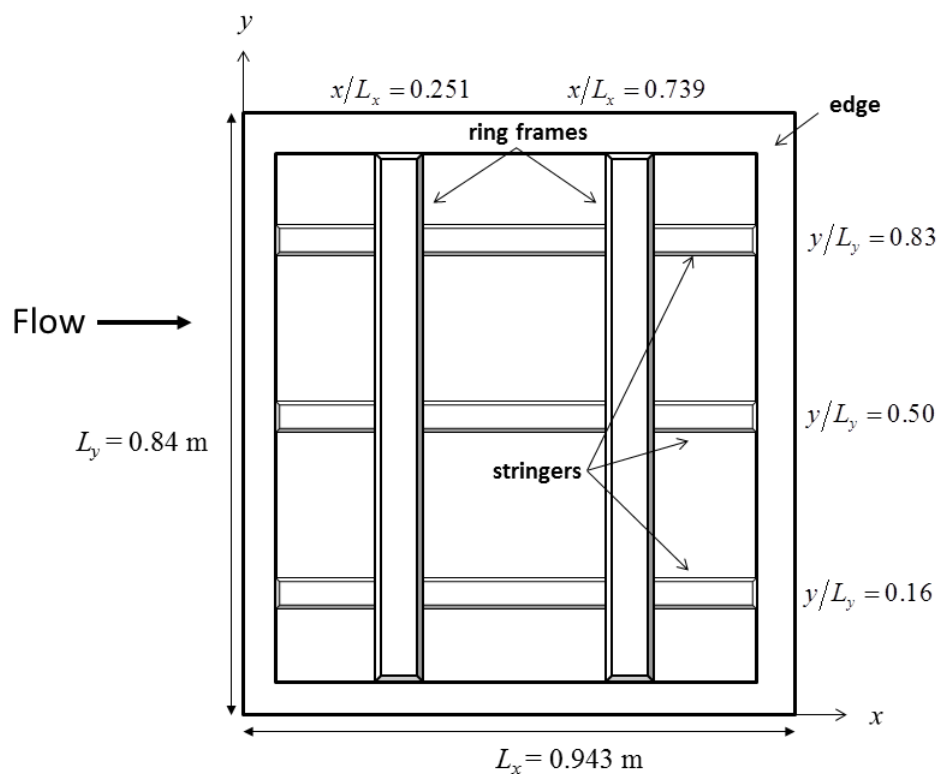


Figure 1: Diagram of the ribbed aircraft panel with two ringframes perpendicular to the flow direction and three stringers parallel to the flow direction.

The ribs have a general “inverted T” shape and are attached to the base plate using spring elements (NASTRAN element CELAS2) with a large stiffness of $1.0E12$ N/m. This is an approximation of a rigid connection. The spring elements are spaced every two inches (5.08 cm) along the length of each rib with two springs across the width of the rib base. The node locations along the surface of the plate and the base of the stiffeners were

Table 2: Dimensions and material properties of the ribbed panel

Streamwise Length	0.9433 m
Spanwise Length	0.84 m
Material Loss Factor	0.01
Young's Modulus	69.0 GPa
Density	2700.0 kg/m ³
Poisson's ratio	0.33

matched so that the springs would connect coincident nodes. The ringframes generally bear more load than the stringers and are therefore larger. Eight notional ringframe and stringer designs were evaluated in the optimization with their respective dimensions and cross-sectional areas listed in Tables 3 and 4 followed by cross-sectional view of each rib (Figs. 2 and 3).

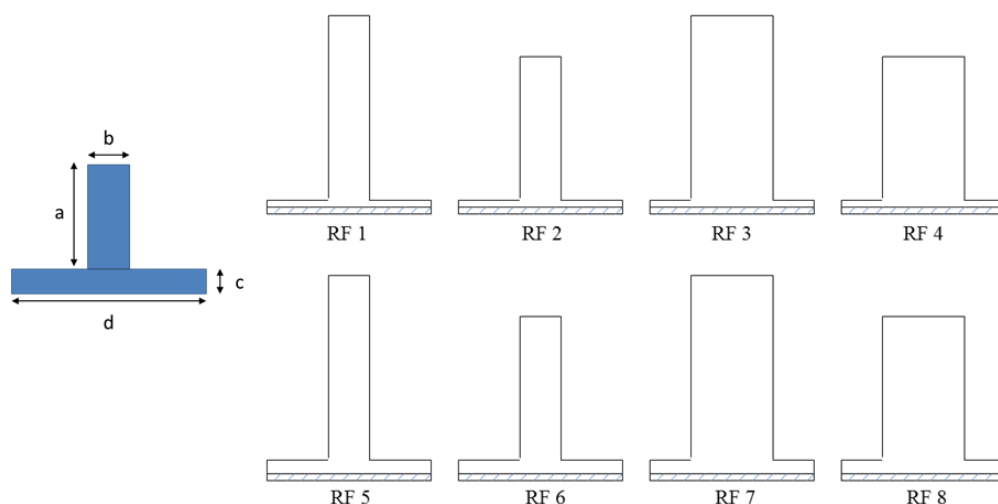


Figure 2: Cross-sectional views of each ringframe design (drawn to proportion). The shaded bottom region represents the base plate. The definitions of the variables a , b , c and d are listed in Table 3.

The cross-sectional design and location of the rib were used as design variables in the optimization. The location of each stiffener was set by assigning individual coordinate systems to each stiffener and varying the coordinate system reference location to a number of pre-set values. Fig. 4 shows the feasible space (constraints on physical location) for each ringframe and stringer. Because the rib locations were not fixed, the crossing point of the frames and stringers was variable. For simplicity, the additional mass caused by the overlapping area between the two stiffeners at the crossing points was ignored.

A boundary element mesh was created using the surface nodes of the plate. The approximate area of each acoustic element is 3.6 mm² except along the edges where the elements are smaller to accommodate the structural mesh. The usable frequency of the mesh is approximately 1 kHz using the six elements per wavelength rule. The modal resistance and reactance matrices were computed in physical space using lumped parameter boundary element approach, (Koopmann and Fahnlne 1997) where each element represents a monopole source since the plate was placed in a rigid baffle. Only outward radiation from the plate was considered so that direct radiation from the ribs, which were

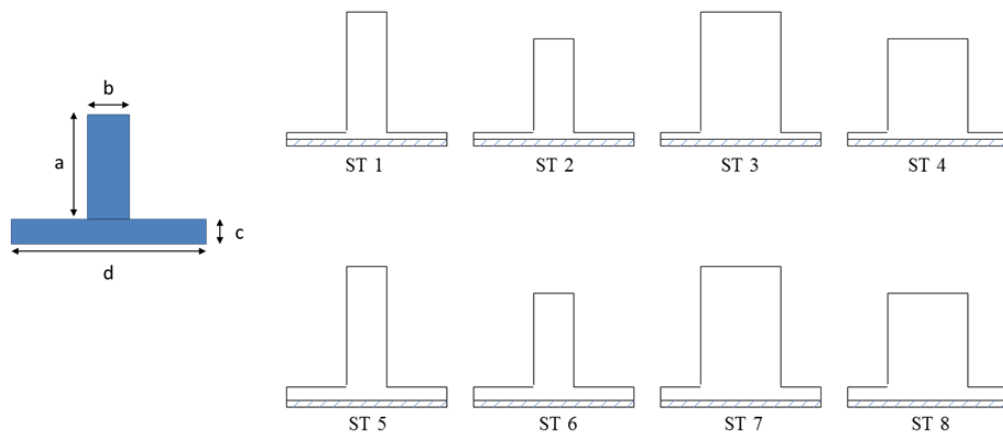


Figure 3: Cross-sectional views of each stringer design (drawn to proportion). The shaded bottom region represents the base plate. The definitions of the variables a , b , c and d are listed in Table 4.

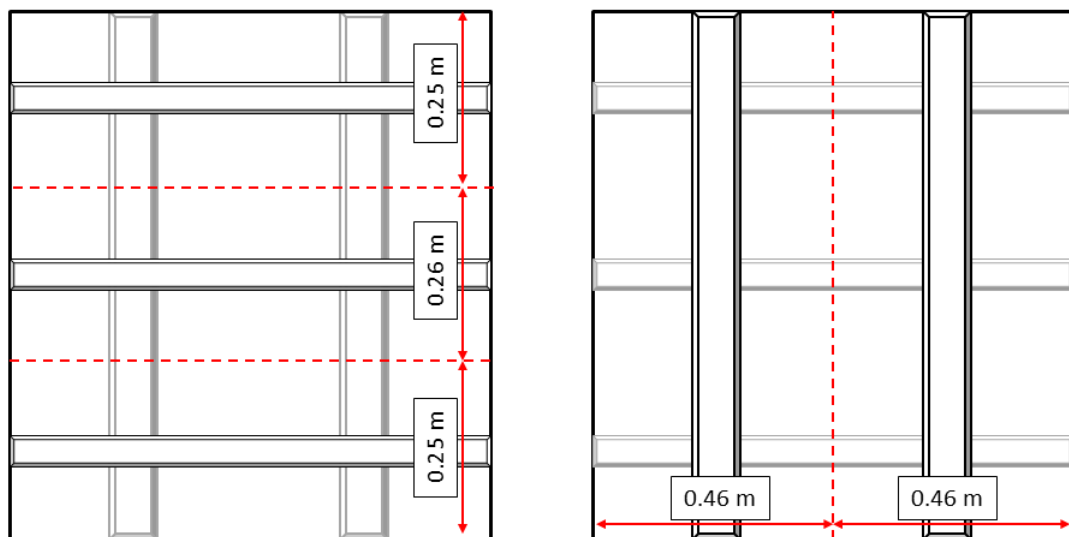


Figure 4: The locations of the ringframe (left) and stringers (right) were allowed to vary during optimization as indicated by the arrows. The dotted lines represent the boundaries between the adjacent stiffeners and are treated as constraints on the ringframe/stringer position.

Table 3: Ringframe dimensions. The cross-sectional area (S_c) and moment of inertia (I) is also listed. The dimensions a, b, c and d are illustrated in Fig. 2.

Ringframe #	a (mm)	b (mm)	c (mm)	d (mm)	S_c (mm ²)	I (mm ⁴)
1	45.0	10.0	1.5	40.41	510.4	1.05E5
2	36.0	10.0	1.5	40.41	420.3	5.7E4
3	45.0	20.01	1.5	40.41	960.5	1.82E5
4	36.0	20.01	1.5	40.41	780.5	9.73E4
5	45.0	10.0	3.0	40.41	570.6	1.31E5
6	36.0	10.0	3.0	40.41	480.6	7.33E4
7	45.0	20.01	3.0	40.41	1020.8	2.13E5
8	36.0	20.01	3.0	40.41	840.7	1.17E5

Table 4: Stringer dimensions. The cross-sectional area (S_c) and moment of inertia (I) is also listed. The dimensions a, b, c and d are illustrated in Fig. 3.

Stringer #	a (mm)	b (mm)	c (mm)	d (mm)	S_c (mm ²)	I (mm ⁴)
1	30.0	10.0	1.5	40.0	360.0	3.49E4
2	24.0	10.0	1.5	40.0	300.0	1.93E4
3	30.0	20.0	1.5	40.0	660.0	5.85E4
4	24.0	20.0	1.5	40.0	540.0	3.17E4
5	30.0	10.0	3.0	40.0	420.0	4.59E4
6	24.0	10.0	3.0	40.0	360.0	2.62E4
7	30.0	20.0	3.0	40.0	750.0	7.23E4
8	24.0	20.0	3.0	40.0	600.0	4.06E4

located on the inward side, was not computed.

To mimic the flight conditions of a typical commercial aircraft, the typical cruise speed and altitude of the Boeing 737 were used to define the flow parameters as listed in Table 5. The cabin pressurization was applied as a static preload of 55 kPa at each base plate element face. Fig. 5 illustrates the pressurization concept with internal and external pressures.

Material damping was included using the complex stiffness matrix \tilde{K} . A DMAP alter script was used to output the complex stiffness matrix directly from NASTRAN in addition to outputting the normal modes. Since a static pressure load was applied, the damping terms in the stiffness matrix are strongly coupled so that modal damping could not be accurately used. Additionally, the static pressure load prohibited the use of component mode synthesis since the substructure basis modes do not respond individually in the same manner as the combined structure. Analysis was performed with sixty structural modes for sound power response up to 500 Hz. Analysis was repeated for several potential designs to ensure that 60 modes was sufficient for accurate modal summation at 500 Hz.

The flow properties were set by the approximate cruise conditions for the Boeing 737. The cruise speed of 216 m/s at 35,000 ft is equal to a Mach speed of 0.7 using the approximate sound speed of 305 m/s. The downstream distance used was 10 m

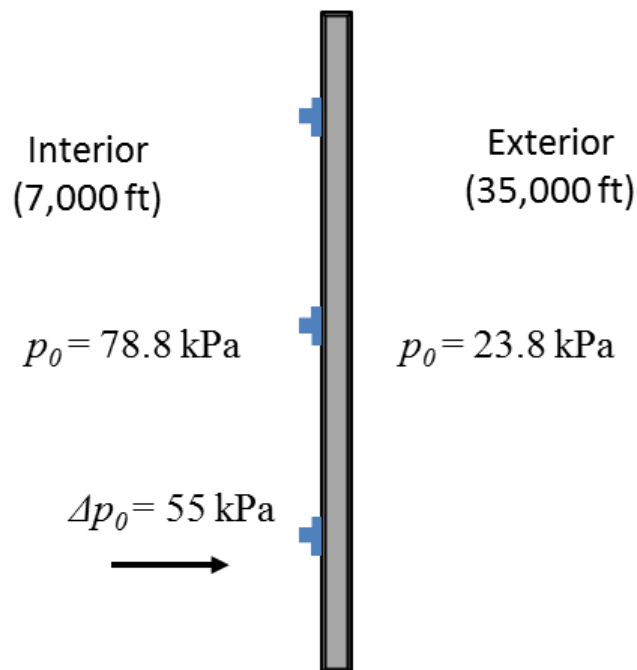


Figure 5: The fuselage of an aircraft is pressurized so that the pressure drop through the panel creates a static load.

representing a passenger seat forward of the wing. Other flow parameters are listed in Table 5 with the resulting point pressure spectrum shown in Fig. 6. Alternate speeds and downstream distances are demonstrated later in this chapter.

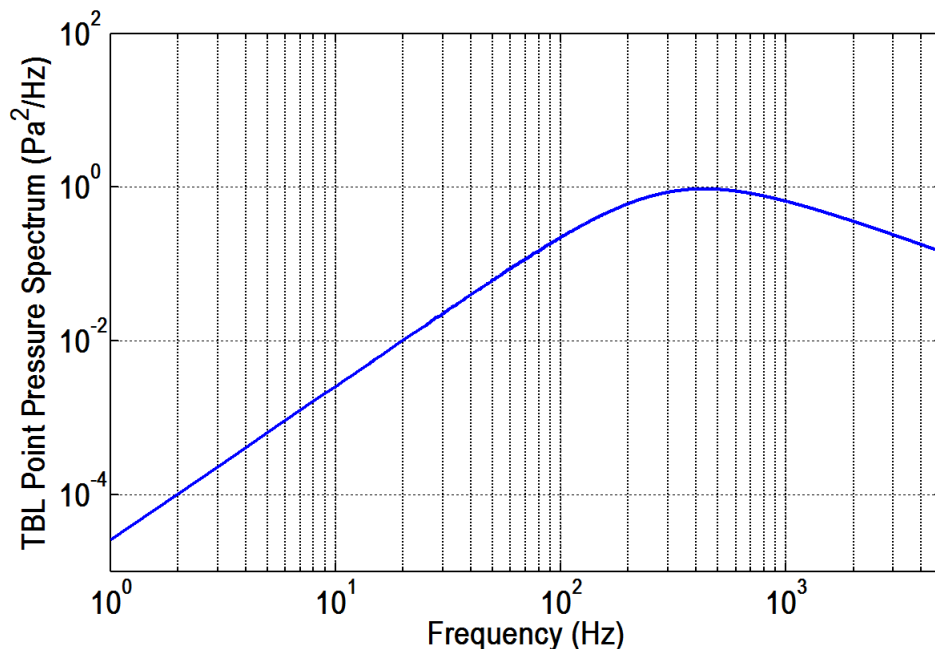


Figure 6: The point pressure spectrum using the Chase-Howe-Lysak model for flow parameters listed in Table 5.

During optimization, the scaled design variables are determined and passed to the objective function. These values are unscaled and then used to assemble the complete FE mesh with the appropriate ribs at the locations specified by the appropriate coordinate system. An eigenvalue problem is solved in NASTRAN to determine the normal modes

Table 5: TBL flow parameters for ribbed panel taken from the cruise conditions of the Boeing 737.

Altitude	35,000 ft
Sound speed (approximate)	305 m/s
Density (ρ)	0.38 kg/m ³
Friction Velocity (u_τ)	6.48 m/s
Free-stream Velocity (U)	216 m/s
Downstream distance (χ)	10 m
Boundary Layer Disp Thickness (δ^*)	1.33E-2 m
Kinematic Viscosity (ν)	3.77E-5
Stream-wise Decay Constant (β_1)	0.07
Span-wise Decay Constant (β_2)	0.7
Turbulence Constant ($\hat{\alpha}$)	0.12

and the matrices are transformed to modal space. The final calculation is performed using the methodology described in Section 2.

4 Results

Structural-acoustic optimization was performed on the panel excited by TBL flow in order to reduce the radiated noise compared to a baseline design. The baseline/initial design was the panel with approximately equispaced ribs (as shown in Figs. 1) and cross-sectional design # 4 for both the ringframes and the stringers. Aircraft panels with equispaced ribs are often used as the starting point for noise reduction studies (see e.g. Refs. (Mejdi and Atalla 2010)).

The optimization was performed on the ribbed panel by varying all ringframe/stringer locations (five design variables) and also the ringframe/stringer cross-sectional designs (two design variables) to reduce the radiated noise. This is a total of seven design variables. The optimized panel has both ringframes and two stringers at the panel edges as shown in Fig. 7. This effectively maximizes the surface area of the center subpanels. The ringframe design is 3 while the stringer is 4 (see Tables 3 and 4). Both cross sections have thin bases (dimension c) and thick stems (dimension d).

The radiated sound power for TBL flow at 216 m/s and a downstream distance of 10 m is shown for the initial and optimized configurations in Fig. 8. The optimized panel has lower radiation above 100 Hz and a total sound power reduction of 9.8 dB, being reduced from 92.9 dB to 83.1 dB (reference to 1e-12 W). The sound power from the optimized panel is also less dominated by individual modes. Increasing the subpanel area decreases its natural frequency which leads to sound reduction since the pressure spectrum amplitude (i.e. the power input to the structure) will be lower, as can be seen in Fig. 6.

5 Conclusion

A structural-acoustic optimization procedure has been presented which can include spatially complex forcing functions and cabin pressurization. The radiated sound power of a TBL-excited, ribbed panel was then minimized by varying the location of the stiffeners.

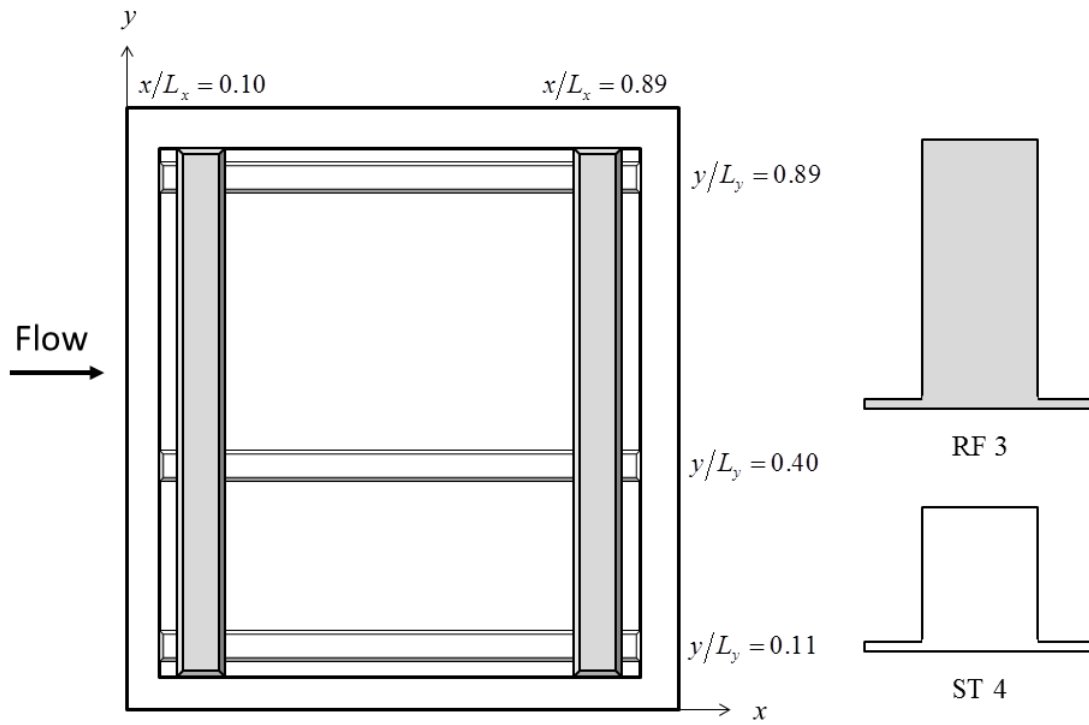


Figure 7: Optimized panel for 216 m/s flow and downstream distance of 10 m. The ringframes are shaded gray while the stringers are white.

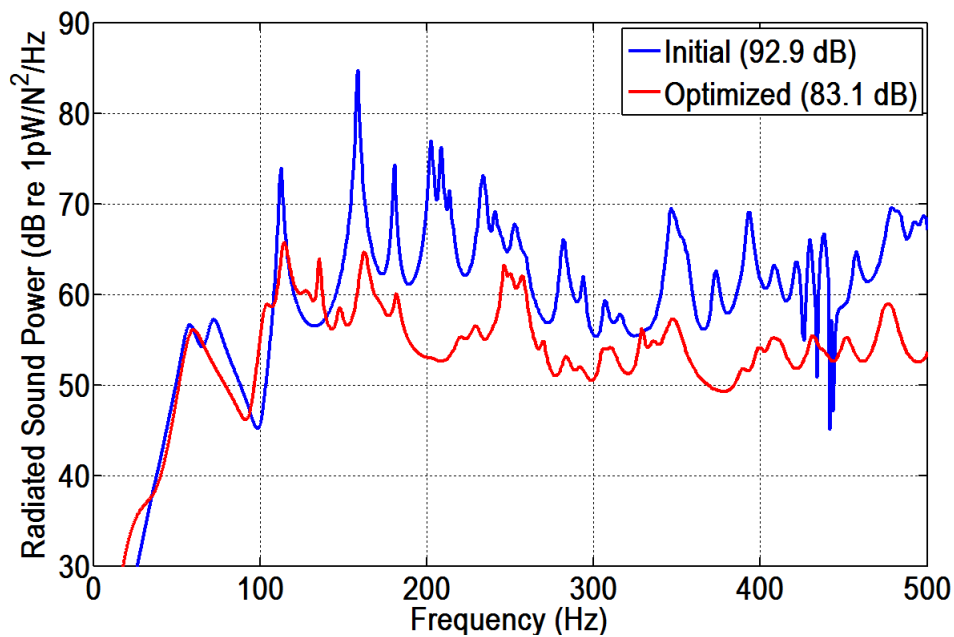


Figure 8: Initial and optimized radiated power for 216 m/s flow and downstream distance of 10 m. The total sound power reduction is 9.8 dB.

The reduction in radiated noise came by pushing the ribs toward the panel edge which leads to less TBL energy excited the structure.

References

- K. Naghshineh, G.H. Koopmann and A.D. Belegundu “Material tailoring of structures to achieve a minimum radiation condition,” *J. Acoust. Soc. Am.* **92**(2), 841–855 (1992).
- W.M. Johnson and K.A. Cunefare “Use of principle velocity patterns in the analysis of structural acoustic optimization,” *J. Acoust. Soc. Am.* **121**, 938–948 (2007).
- A.D. Belegundu, R.R. Salagame and G.H. Koopmann “A general optimization strategy for sound power minimization,” *Struct. Opt.* **8**(2–3), 113–119 (1994).
- S. Marburg, F. Dienerowitz, D. Fritze and H.J. Hardtke “Case studies on structural-acoustic optimization of a finite beam,” *Acta Acustica united with Acustica* **92**(3), 427–439 (2006a).
- A. Powell “On the fatigue failure of structures due to vibrations excited by random pressure fields,” *J. Acoust. Soc. Am.* **30**(12), 1130–1135 (1958).
- A. Mejdji A. and N. Atalla “Dynamic and acoustic response of bidirectionally stiffened plates with eccentric stiffeners subject to airborne and structure-borne excitations,” *J. Sound and Vib.* **329**, 4422–4439 (2010).
- S.A. Hambric, D.A. Boger, J.B. Fahline and R.L. Campbell “Structure- and fluid-borne acoustic power sources induced by turbulent flow in 90° piping elbows,” *J. Fluids Struct.* **26**, 121–147 (2010).
- P. Joshi, S.B. Mulani, W.C.H. Slemp and R.K. Kapania “Vibro-acoustic optimization of turbulent boundary excited panel with curvilinear stiffeners,” *J. Aircraft* **49**(1), 52–65 (2012).
- M.R. Shepherd and S.A. Hambric “Minimization of the acoustic power radiated by a fluid-loaded, curved panel excited by turbulent boundary layer flow,” *J. Acoust. Soc. Am.* **136**(5), 2575–2585 (2014).
- M.R. Shepherd and S.A. Hambric “An approach for Structural-acoustic optimization of ribbed panels using component mode synthesis,” *Proceedings of Internoise 2012/ASME NCAD IN12-592* (2012).
- J.S. Bendat and A.G. Piersol *Random Data*, Wiley, New York, 263 (2000).
- G.H. Koopmann and J.B. Fahline *Designing Quiet Structures: A Sound Power Minimization Approach*, Academic Press, San Diego, London, 1–244 (1997).
- P.D. Lysak “Modeling the wall pressure spectrum in turbulent pipe flows,” *J. Fluids Eng.* **128**, 216–222 (2006).
- G.M. Corcos “Resolution of pressure in turbulence,” *J. Acoust. Soc. Am.* **35**(2), 192–199 (1963).
- R.H. Mellen “On modeling convective turbulence,” *J. Acoust. Soc. Am.* **88**(6), 2891–2893 (1990).

N. Hansen “An analysis of mutative σ -self-adaptation on linear fitness functions,” *Evol. Comp.* **14**(3) 255–275 (2006).